On the dissolution kinetics during acid pickling and Zr-based conversion coating of aluminum alloys using element-resolved electrochemistry

B. Bin Mohamad Sultan, D Persson, Dominique Thierry, Junsoo Han, Kevin Ogle

On the dissolution kinetics during acid pickling and Zr-based conversion coating of aluminum alloys using element-resolved electrochemistry

B. Bin Mohamad Sultan[1,2,3,4], D. Persson[3], D. Thierry[3], J. Han[4], K. Ogle[1,*]

[1]Chimie ParisTech, PSL Research University, Institut de Recherche Chimie-Paris CNRS, Paris, France
[2]*Institut de la Corrosion* (French Corrosion Institute), Brest, France
[3]Research Institutes of Sweden (RISE), Kista, Sweden
[4]*Sorbonne Université*, CNRS, *Laboratoire Interfaces et Systèmes Électrochimiques* (LISE), Paris, France

b.bin-mohamad-sultan@chimieparistech.psl.eu
dan.persson@ri.se
dominique.thierry@ri.se
junsoo.han@sorbonne-universite.fr
kevin.ogle@chimieparistech.psl.eu*

*Indicates the corresponding author

Abstract

The acid pickling of Al-3at.%Mg, Al-3at.%Cu, and aluminum alloy (AA) 7449-T651 in nitro-sulfuro-ferric acid was investigated using element-resolved electrochemistry (AESEC) in terms of their elemental dissolution kinetics. The influence of this acid pickling on the subsequent Zr-based conversion coating process was also demonstrated on these alloys by monitoring the dissolution rates of the alloying elements during conversion and the final elemental depth profiles from calibrated glow discharge-optical emission spectroscopy (GD-OES). The separate influence of fluoride (F^-) and nitrate (NO_3^-) as additives on the dissolution kinetics was also investigated when added to the conversion coating bath solution. F^- increased the dissolution rate of Al but no significant effect was seen on Cu, while NO_3^- enhanced the dissolution rates of both elements. Fourier-transform infrared reflection absorption spectroscopy (FT-IRRAS) data suggested a greater Zr-fluoride presence if the conversion coating was performed on a non-acid-pickled surface.

1) Introduction

The integration of aluminum alloys (AA) in various parts and components of aerospace applications is prevalent due to their combined lightweight and high-strength properties. Nonetheless, aluminum alloys are also known to be relatively susceptible to corrosion, especially the alloy series that are widely used in the aerospace industry (AA2000s and AA7000s) which are prone to intergranular corrosion and lead to reduced lifespan of the parts [1]. Therefore, various surface treatments have been developed to improve the corrosion resistance of aluminum alloys and address this issue. One such treatment is conversion coating where thin oxide films are deposited on the metallic substrate's surface to enhance paint adhesion mainly and to lower the electrochemical activity of the interface metal-oxide-polymer [2–4].

Conventionally, Cr(VI)-based conversion coatings were the most commonly used due to their excellent performance and relatively low cost [1,2,5,6]. However, due to recent legislative and regulatory amendments, Cr(VI)-free formulations have been sought after [1,2,7–9]. Generally, those newer treatments are reported to be much more sensitive to the material's surface chemistry and thus render the application delicate on surfaces that are complex in terms of phases and elements [2]. Therefore, pretreatment is often required which should ideally transform the different surfaces into equivalent ones for the subsequent conversion coating application [1,2,10]. Nonetheless, the Zr-based conversion coating is a promising candidate to replace the chromate-based conversion coating [5,6].

The Zr-based conversion coating (ZrCC) is an electrochemically driven process involving a mixed-potential process similar to corrosion. The actual deposition mechanisms are complex [2]. In the current understanding and in the simplest form, it involves the surface activation, nucleation, and growth phases. The activation phase occurs mainly through the removal of the pre-existing oxides by free F^- ions and, to a smaller extent, by hexafluoro-zirconate [1,6]. Then the nucleation phase revolves around the precipitation or hydrolysis of the hexafluoro-zirconate ions at localized cathodic sites such as intermetallic particles where generation of hydroxide may take place. The formation of hydroxide may originate from reactions of hydrogen evolution, oxygen reduction, and/or reduction of other oxidizing species leading to local pH increase and prompting the deposition of insoluble species of Zr-oxide/hydroxide. After the preferential precipitation at the cathodic sites, the oxide deposition continues laterally during the growth phase. For a more detailed and thorough explanation of these mechanisms, readers are invited to consult the excellent reviews by Milošev[6] and by Becker[11] on this subject.

A typical Zr-conversion coating bath solution may have additives fulfilling various roles. Organic additives may be included to improve subsequent polymer coating while inorganic additives such as F^-, Cu(II), and NO_3^- have been reported to affect the kinetics of film formation or influence the final film structure [1,2,5,7,12,13]. For example, Han *et al.* reported that the addition of NO_3^- in the Zr-conversion coating bath solution served to increase hydroxide formation and resulted in greater ZrO_2 deposition on a Zn-Al-Mg alloy coating while Cu ion from the bath solution was reduced on the surface through displacement reaction and served as micro-cathodes [2], with the latter finding was also reported by Cerezo *et al.* [14]. Although NO_3^- is commonly added to increase the electrolyte's oxidative power, it is known to promote passivation on Al [15]. Increasing the concentration of free F^- ions was mentioned to increase the conversion rate [1], since it enhances the dissolution of Al-based pre-existing oxides and improves the reactivity of metallic Al with the oxidizing agents in the formulation due to the enhanced solubility of hexafluoroaluminate species.

Although one of the main advantages of ZrCC is the possibility of its application to a wide range of metallic substrates including aluminum alloys, the final efficiency depends on many factors such as the superficial presence of various phases and different elemental components [2,7]. This renders the understanding of the interactions between conversion coating bath solution components and the different elements constituting the bulk substrate crucial for any intelligent development of surface treatment solutions. Briefly, a conversion coating bath solution should be able to induce two phenomena on the surface of the metallic substrate ─ the oxidation of the surface resulting in the dissolution of metallic elements and the deposition of insoluble metal-oxides through, in the case of ZrCC, pH-induced precipitation. These two phenomena are related and dependent on each other [6].

Since the Zr conversion process functions *via* a dissolution-precipitation mechanism, the goal of this work is to disentangle the dissolution and precipitation phenomena using AESEC to directly measure the elemental dissolution rates *in situ* and GD-OES to quantify the extent of the resulting precipitation *ex situ*. The state of the surface after conversion coating was further characterized by FT-IRRAS. This methodology was applied to determine how the dissolution and precipitation reactions were affected by:

a. the elemental composition on the surface of the substrate with and without prior acid pickling (nitro-sulfuro-ferric solution)
b. the presence of additives in the bath formulation (F^- or NO_3^- ions).

2) Experimental

The alloys used in this work were foils of Al-2.5wt.%Mg (A5052, 0.5 mm thickness, denoted as Al-3at.%Mg herein), Al-6wt.%Cu (AA2219, 0.125 mm thickness, denoted as Al-3at.%Cu herein), supplied by Goodfellow, product number AL210350/1 and AD220212/1; batch number 300926490 and 300926491, respectively. These alloys were selected for this work because they represent one of the simplest compositions of Al alloys. Substrates of AA7449-T6531 were also used to represent complex Al alloy. The nominal compositional information of each alloy as given by the manufacturer is shown in Table 1.

Table 1 Nominal bulk elemental composition of the aluminum alloys in weight and atomic percentages.

Alloy	Composition	Al	Cu	Mg	Zn	Mn	Fe	Ti
Al-3at.%Mg (AA5052)	wt.%	97.5		2.50				
	at.%	97.2		2.77				
Al-3at.%Cu (AA2219)	wt.%	92.3	7.70			0.30	0.03	0.06
	at.%	96.6	3.42			0.15	0.02	0.03
AA7449-T651	wt.%	87.3	1.87	2.16	8.24	0.03	0.07	0.03
	at.%	92.8	0.84	2.55	3.61	0.02	0.04	0.02

The samples were cut and manually ground under ethanol with SiC papers to a final finish of P2400. The grindings were necessary to ensure a relatively consistent and comparable surface from one specimen to another by minimizing any surface contaminant, rolling mark, and grain-refined surface layer [16].

The solutions were prepared using reagent-grade chemicals and deionized water (18.2 MΩ cm) purified by a Millipore™ system. The acid pickling solution was prepared to be 2.8 N of mixed acid at the equinormal contribution of nitric and sulfuric acids, with 0.2 M Fe(III) as an additive. This nitro-sulfuro-ferric acid pickling solution is denoted NSFe herein. The synthetic conversion coating solutions were prepared with 0.76 g L^{-1} of H_2ZrF_6 (45 wt.%) electrolyte as a base representative of the ZrCC. The pH of the prepared solutions was adjusted to 4.0 by adding 1 M NaOH dropwise. A comparison between this synthetic conversion bath formulation and a similar commercial one was made *via* FT-IRRAS to ensure that the former is sufficiently representative of the latter as shown in Annexes (Figure). It should be noted that the

commercial conversion formulation contains a low content of silane, which is also present in the coating layer treated with this solution. As for the synthetic formulation used herein, the additives 50 mM F^- and 100 mM NO_3^- were added separately as NaF and $NaNO_3$ respectively. Solutions of 50 mM NaF and 100 mM $NaNO_3$ were also prepared, and the pH adjusted to 4.0 by adding H_2SO_4 dropwise.

a) Atomic emission spectroelectrochemistry (AESEC)

AESEC is an element-resolved electrochemical technique that has been extensively detailed elsewhere [17,18]. Essentially, it involves an electrochemical flow cell outfitted with a three-electrode system linked to an inductively coupled plasma-atomic emission spectrometer (ICP-AES). This setup enables the simultaneous acquisition of elemental dissolution rates and electrochemical response *operando*. The determination of elemental concentrations over time relies on analyzing atomic emission intensity from the plasma at various characteristic wavelengths. The ICP-AES instrument utilized, a Horiba Jobin Yvon Ultima 2C, features a Paschen-Rungen type polychromator with a 50 cm focal length, equipped with an array of photomultiplier tube detectors at specific wavelengths, alongside a monochromator with a 1 m focal length [19]. Table 2 recaps the different detection limits (defined as three times the standard deviation of the background intensity signals, $C_{3\sigma}$) of different wavelengths found in the various solutions used in this study.

Table 2 Characteristic emission wavelengths and typical detection limits of the ICP-AES for various elements under the conditions of the experiments. The detection limits are expressed in the ppb (and in brackets as an equivalent rate, nmol s^{-1}).

↓Solution/ → Element (wavelength, nm)	Al 396.15	Cu 324.75	Mg 279.08	Zn 213.86
NaF 50mM	24 ($4x10^{-2}$)	2 ($1x10^{-3}$)	1 ($1x10^{-3}$)	
NaF 100mM	26 ($4x10^{-2}$)	3 ($2x10^{-3}$)	0.2 ($4x10^{-4}$)	
$NaNO_3$ 50mM	82 ($1x10^{-1}$)	2 ($1x10^{-3}$)	0.4 ($7x10^{-4}$)	
$NaNO_3$ 100mM	26 ($4x10^{-2}$)	3 ($2x10^{-3}$)	0.2 ($4x10^{-4}$)	
NSFe	43 ($6x10^{-2}$)	40 ($2x10^{-2}$)	7 ($1x10^{-2}$)	96 ($6x10^{-2}$)
ZrCC	63 ($1x10^{-1}$)	4 ($3x10^{-3}$)	0.4 ($6x10^{-4}$)	4 ($3x10^{-3}$)
ZrCC+ NaF 50 mM	67 ($1x10^{-1}$)	2 ($2x10^{-3}$)	2 ($3x10^{-3}$)	
ZrCC+ $NaNO_3$ 50 mM	109 ($2x10^{-1}$)	3 ($2x10^{-3}$)	0.3 ($6x10^{-4}$)	

The temperature of the electrolyte was controlled with a water bath system and the temperature of the alloy specimen was maintained with a hollow copper block where the water from the bath was circulated through the hollow copper block to maintain thermal transfer at 50 °C. The copper block was also kept electrically insulated from the sample with the help of cellulose tape. The electrolytes are naturally aerated.

The three-electrode electrochemical system employed a saturated calomel electrode as the reference and a thin Pt foil as the counter electrode, connected to a potentiostat (Gamry Reference 600™). Open circuit potential experiments (OCP) were performed for at least 10 min, and each experiment was repeated at least twice.

b) Surface characterization

GD-OES was used to probe the elemental depth profiles of the substrates before and after different surface treatments. The instrument has been calibrated using standard materials to be able to transform elemental depth profiles from signal intensity over time to elemental composition (in atomic percentage) as a function of depth (in micrometers). Calibrated elements

are Al, Cu, Mg, Fe, Mn, O, Zn, and Zr. However, F was not calibrated due to the instrument's limitation, which uses Ar gas as the sputtering agent.

FT-IRRAS was performed using a Bruker Vertex 70™ spectrometer with a Hyperion 3000™ microscope (Bruker Optics, Ettlingen, Germany) equipped with a broad band mercury cadmium telluride (MCT) detector. FT-IRRAS measurements were made using a grazing angle objective (Bruker) and p-polarized light. A gold mirror was used to record background spectra. Spectra were acquired in the region 500 to 4000 cm^{-1} by adding 1000 scans at 8 cm^{-1} resolution.

c) Data treatment

The data treatment of AESEC is similar to that of previous papers [20,21]. The raw elemental intensities during the experiment, I_λ, were transformed into elemental dissolution rates of the element M of the alloy specimen (v_M) in nmol s^{-1} by utilizing the following formula:

$$v_M = \frac{f(I_\lambda - I^\circ_\lambda)}{M_M \, \kappa_\lambda} \qquad \textit{Equation (1)}$$

with f as the flow rate of the electrolyte through the reactional compartment, I°_λ as the background intensity, κ_λ as the sensitivity factor of the corresponding wavelength, and M_M as the molar mass of the dissolved ion species. The elemental dissolution rates can also be expressed as elemental equivalent current (i_M) in A by applying Faraday's law:

$$i_M = z_M \, v_M \, F \qquad \textit{Equation (2)}$$

As for the calibrated GD-OES data, the average deposited quantity of an element M ($\langle q_M \rangle$, in atomic percent) is calculated *via* the following equation:

$$\langle q_M \rangle = \frac{\int_0^{x_{max}} q_M(x) \, dx}{x_{\max}} \qquad \textit{Equation (3)}$$

Where x_{max} presents the maximum depth sputtered or analyzed, and $q_{M(x)}$ the atomic percentage of the same element as a function of depth x.

3) Results and discussion

a) Al-3at.%Mg

The Al-3at.%Mg alloy was subjected to different surface treatment sequences (acid pickling and/or conversion coating) while the corresponding dissolution reaction was monitored *via* AESEC. At the end of these surface treatments, the surfaces were further characterized by elemental depth profiling using calibrated GD-OES. The pickling solution was 2.8 N equinormal mix of nitric and sulfuric acids with the addition of 0.2 M of Fe(III), while the ZrCC bath solution was an in-house prepared solution of 760 ppm of H_2ZrF_6 at pH 4.0. Both the acid pickling and the conversion coating processes were performed at 50 °C. Figure 1 shows the compilation of results obtained when a bare (but ground to P2400 finish) Al-3at.%Mg alloy surface was subjected to acid pickling in nitro-sulfuro-ferric acid (NSFe). Al-3at.%Mg subjected to ZrCC bath solution is also included without (ZrCC) or with (NSFe-ZrCC) prior acid pickling of the surface. Also shown within the same figure are the elemental depth profiles obtained before any reaction on the surface (bare, denoted as 0) as well as after AESEC analyses of different surface treatments as mentioned previously.

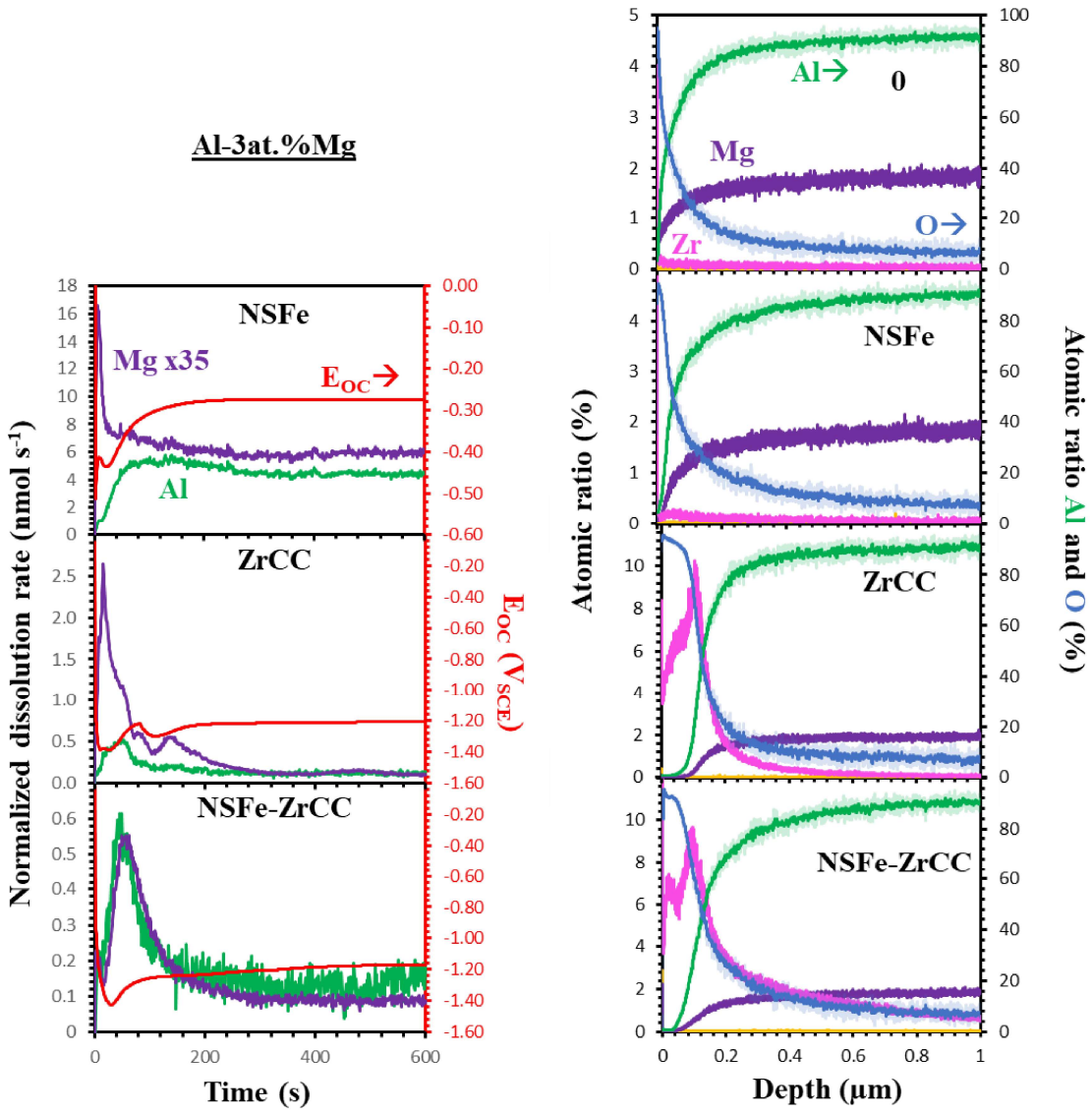

Figure 1 Left column: Normalized AESEC dissolution profiles of Al-3at.%Mg during acid pickling and the corresponding open circuit potential variation as a function of time during different surface treatment steps — during nitro-sulfuro-ferric (NSFe) acid pickling, and during Zr-conversion coating of bare (ZrCC) and benchtop acid pickled (NSFe-ZrCC) surfaces. Right column: Calibrated GD-OES elemental depth profiles of the corresponding surfaces after each surface treatment step compared with the bare surface (denoted as 0). Note that the atomic percentage of surface Al and O is given on the right-hand y-axes.

The dissolution profiles demonstrate that Mg underwent a sharp peak of selective dissolution as soon as the pickling solution came in contact with the substrate. The dissolution of Mg reached a peak very early at the beginning of the experiment before subsiding, as is usually the case for this combination of Mg and Al, while the dissolution of Al peaked later [21]. The selective dissolution of Mg was sustained throughout the whole experiment without turning into congruent dissolution, unlike the case for the same alloy in sulfuric and nitric acids (see

reference [21]). Repeating the same experiment produced a similar result (not shown here), therefore this peculiarity is not a one-off occurrence. The GD-OES depth profile of Mg (Figure 2) after the acid pickling treatment differs only slightly as compared to the surface before the pickling treatment (bare). The corresponding potential variation (Figure 1) showed, initially, an anodic dip where peak and valley trends are seen similar to the ones observed in other cases when this alloy was subjected to ferric species containing acid pickling solutions ([21]).

During ZrCC processes (Figure 1), the oxidation or dissolution rate of the elements in question was an order of magnitude less than that seen during acid pickling. Nevertheless, when subjected to the conversion coating bath solution (ZrCC), the bare surface demonstrated an initial selective dissolution and peaking of Mg relative to Al, before reaching a congruent dissolution rate with Al after around 300 s. The excess Mg dissolution was eliminated when the ZrCC treatment followed acid pickling (NSFe-ZrCC) with nitro-sulfuro-ferric acid (NSFe) as Al and Mg dissolution were congruent from the beginning of the process and seemed to be sustained almost to the end. Although the rates of Al dissolution seemed to be of similar value in both cases, the dissolution rates for Mg, on the other hand, were reduced for the first 300 s on the acid pickled surface, possibly due to the slight surface depletion of Mg resulting from the prior acid pickling process (this depletion was slightly apparent *via* GD-OES analyses). The open circuit potentials for both cases seemed similar in value, especially after 300 s when they leveled off around -1.2 V_{SCE}.

GD-OES profiles after ZrCC processes revealed the presence of a significantly higher amount of Zr and an elevated quantity of O (Figure 2). The presence of Zr remained elevated compared to the background level (from the non-conversion coated surfaces of 0 and NSFe) down to 200 nm for the ZrCC case and even deeper for the NSFe-ZrCC case. Comparing the thicknesses reported in the literature, a thickness of between 30-100 nm is expected for a typical Zr-based conversion layer on Al alloy [1,7], with even a thickness of 140 nm being possible [12], therefore the results from GD-OES are indeed surprising. A highly diffuse layer and the imperfect sputtering of Zr during the GD-OES analyses, and even simply how the “thickness” is defined might be the factors for this.

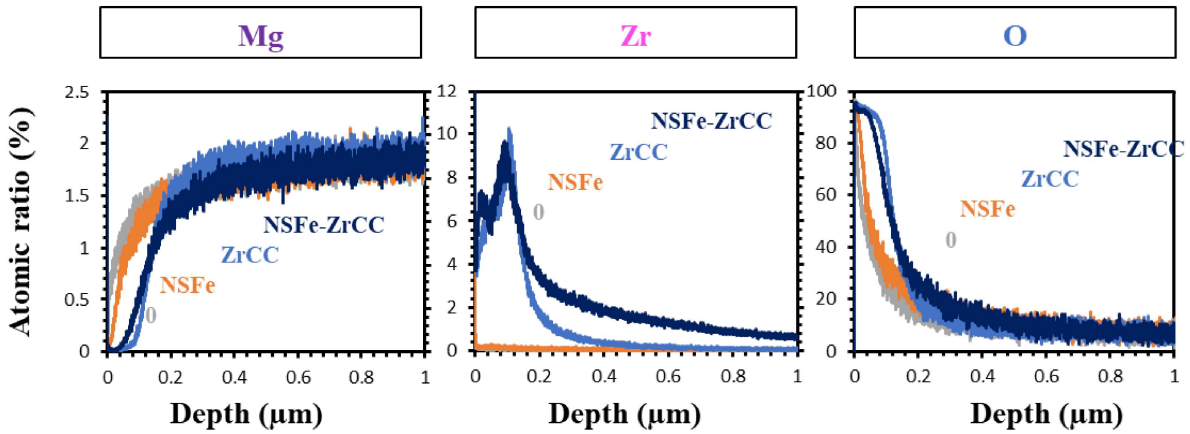

Figure 2 Calibrated individual elemental GD-OES depth profiles of Mg, Zr, and O of the surfaces after each surface treatment step superposed together for easier comparison of Al-3at.%Mg. For reference, 0 denotes bare surface, NSFE signifies surface after acid pickling in nitro-sulfuro-ferric acid, ZrCC refers to bare surface after Zr-conversion coating, and NSFe-ZrCC represents NSFe surface after Zr-conversion coating.

Note that the detection and accurate quantification of F was not possible by the GD-OES available for this study since it necessitates the use of Ne gas instead of Ar as a sputtering agent [22]. Nonetheless, the nature of the Zr-rich layer is believed to be bi- or tri-layer consisting of oxides and fluorides of Zr from the literature [6,12].

b) Al-3at.%Cu

A series of similar experiments and analyses regarding surface treatments were equally performed on Al-3at.%Cu alloy similar to those performed on Al-3at.%Mg and the results are shown in Figure 3.

During acid pickling of Al-3at.%Cu in nitro-sulfuro-ferric acid, Cu underwent selective dissolution throughout the experiment like the case with Mg in Al-3at.%Mg alloy, and exhibited a trend not unlike those seen in the previous paper when Al-3at.%Cu is exposed to a NO_3^--containing acid solution [21]. The dissolution rate of Cu also peaked around the same time frame as that of Al before subsiding through the rest of the pickling treatment. This selective dissolution of Cu and therefore its surface depletion was also apparent in the GD-OES depth profiling analyses. A significant reduction in the proportional quantity of Cu was demonstrated after the acid pickling treatment as compared to the bare surface.

Whereas during ZrCC reactions, the dissolution rates of Cu were approximately two orders of magnitude lower than during acid pickling. In fact, the dissolution of Cu was only expected due

to the presence of dissolved oxygen and through the attack of free F^- ions in the bath solution [23–25]. The rates of Al dissolution were comparable after around 300 s during the conversion process, although at the beginning of the reaction, the rate was higher (almost double) on the surface with prior acid pickling treatment, an observation attributed to the fact that superficial Cu had been depleted after the first pickling process and therefore the surface availability of Al was enhanced.

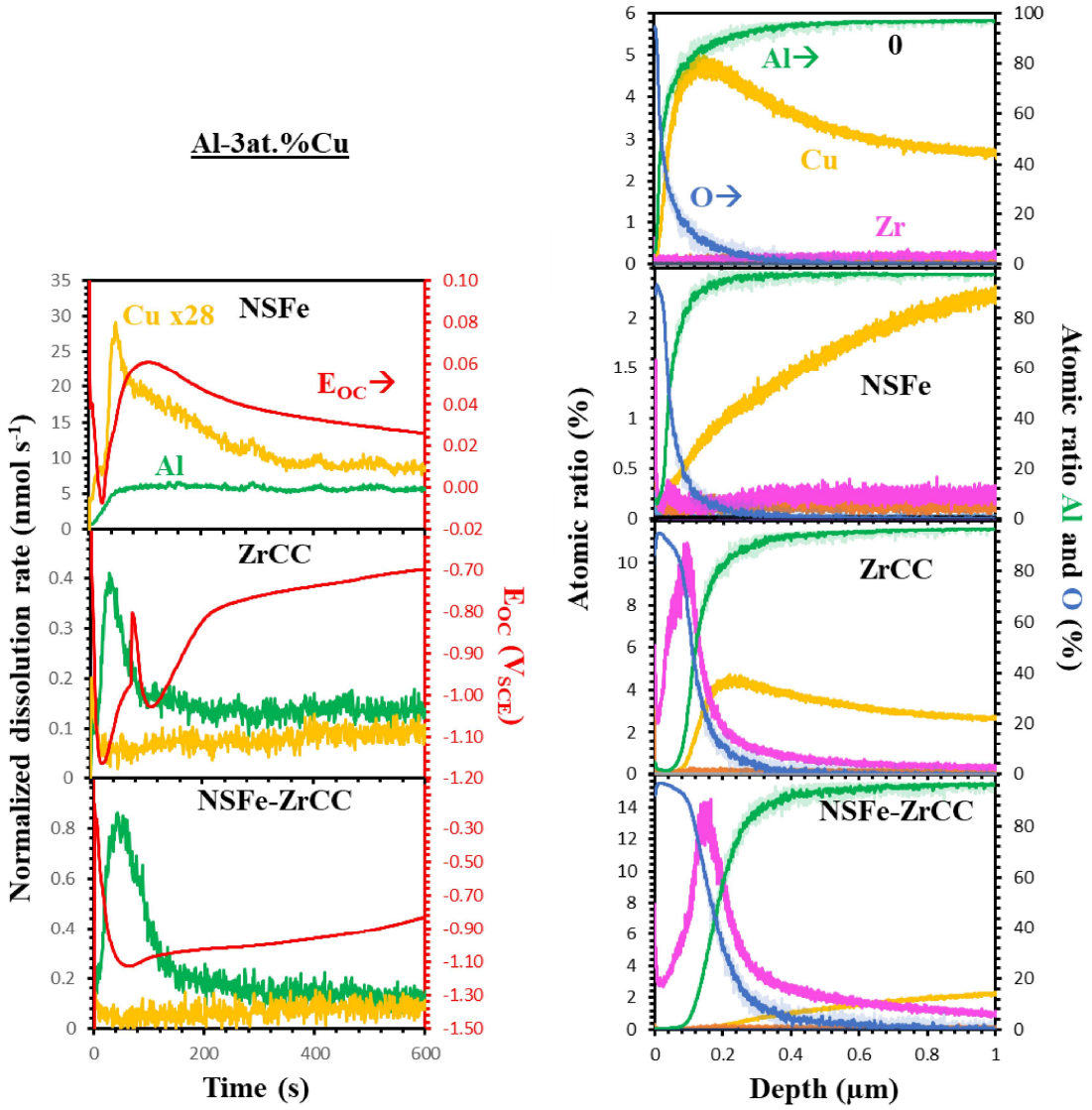

Figure 3 Left column: Normalized AESEC dissolution profiles of Al-3at.%Cu during acid pickling and the corresponding open circuit potential variation as a function of time during different surface treatment steps — during nitro-sulfuro-ferric (NSFe) acid pickling, and during Zr-conversion coating of bare (ZrCC) and benchtop acid pickled (NSFe-ZrCC) surfaces. Right column: Calibrated GD-OES elemental depth profiles of the corresponding surfaces after each surface treatment step compared with the bare surface (denoted as 0). Note that the atomic percentage of surface Al and O is given on the right-hand side y-axes.

The contrast in the quantity of Cu is also apparent from the elemental depth profiling analyses after conversion coating. The quantity of Zr appeared to be slightly higher and extended deeper on the surface that had undergone acid pickling before the conversion process compared to the bare surface that was conversion coated.

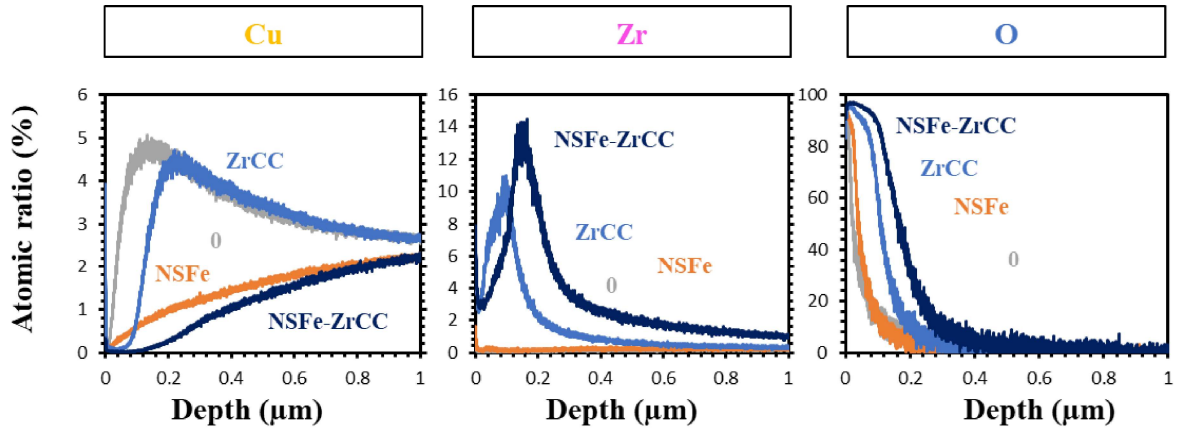

Figure 4 Calibrated individual elemental GD-OES depth profiles of Mg, Zr, and O of the surfaces after each surface treatment step superposed together for easier comparison of Al-3at.%Cu. For reference, 0 denotes bare surface, NSFe signifies surface after acid pickling in nitro-sulfuro-ferric acid, ZrCC refers to bare surface after Zr-conversion coating, and NSFe-ZrCC represents NSFe surface after Zr-conversion coating.

The kinetic of conversion layer growth on the surface of Al-3at.%Cu was followed through FT-IRRAS measurement after conversion treatment at increasing durations. The investigated states of the surface before the conversion coating were bare mirror-polished, pre-treated with sulfuric acid pickling, and pre-treated with nitric acid pickling. Figure 5 shows the FT-IRRAS curves obtained *ex situ* after ZrCC process with different treatment times along with the corresponding growth profile for select wavenumbers showing the rate of formation of different surface films or deposits.

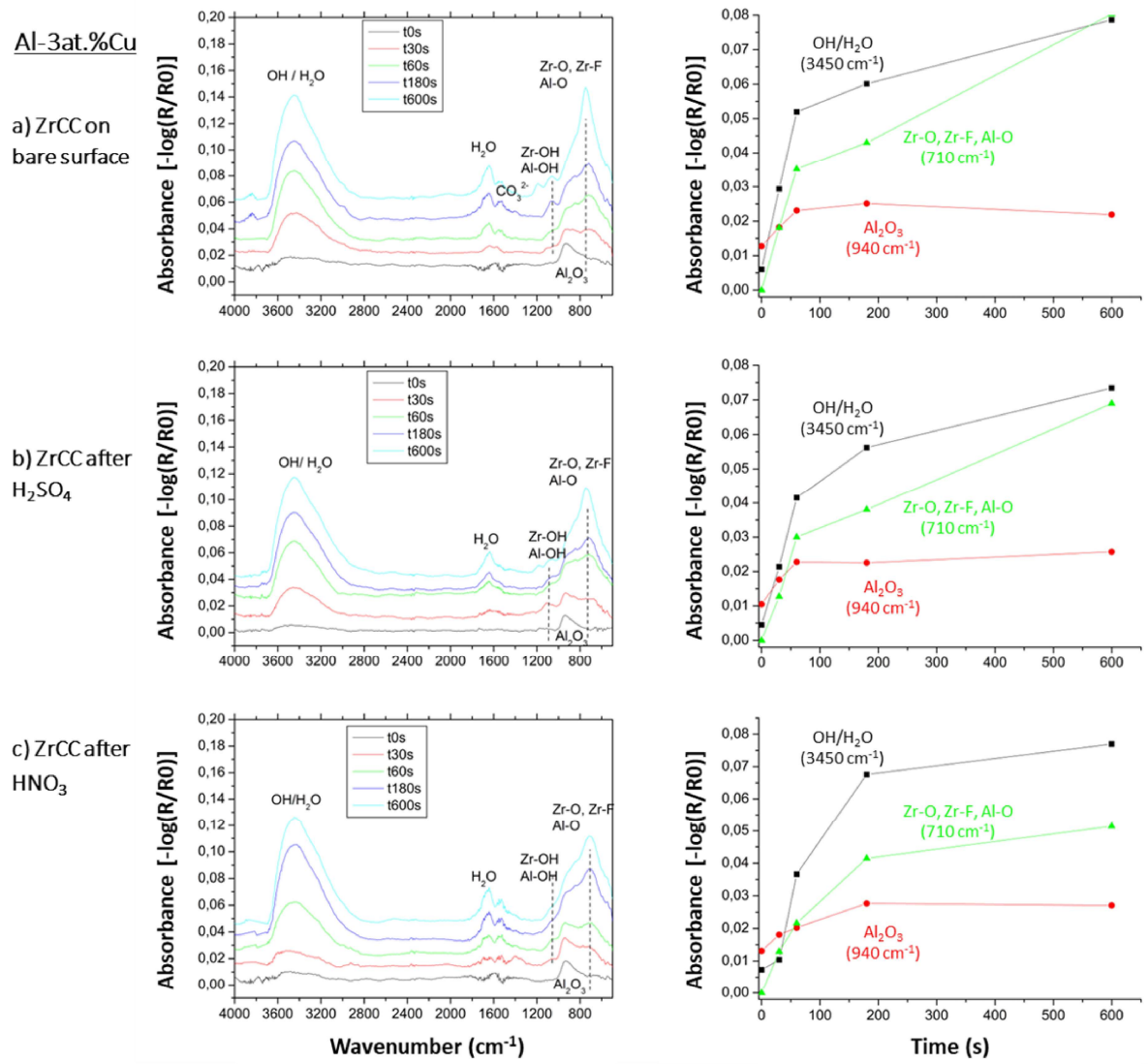

Figure 5 Left: FT-IRRAS data showing the curves obtained after conversion coating with ZrCC on different surfaces of Al-3at.%Cu at different durations. The bands have been assigned by referencing literature values. Right: The corresponding increase in intensity for select wavenumbers as a function of treatment duration.

The FT-IRRAS data shows overall comparable profiles in all cases, with only the intensity of certain bands being different. This means that the nature of the deposited films was similar, but the percentages of the composition may differ. Longer conversion coating treatment also leads to greater intensity for the prominent bands, except for the one attributed to Al_2O_3 which ceased to increase after 180 s. Curiously, the bands assigned to OH/H_2O and mixed oxide-fluoride (Zr-O, Zr-F, Al-O) were measured to have higher intensity after ZrCC treatment on the bare surface compared to the acid-pickled ones, inconsistent with the results obtained from GD-OES where the intensity of Zr and O were greater on the acid-pickled surface. Nevertheless, the GD-OES

findings did not consider the influence of F^- and molecular water present either within or on the film, which could potentially explain this disparity. Thus, the conversion coating on the non-acid pickled surface can be expected to result in a greater F^- insertion compared to the acid-pickled ones. In any case, the formation rate of the films on all three surfaces is greatly reduced after 180 s if not ceased altogether as was the case for Al_2O_3.

c) AA7449-T651

Both the Al-3at.%Mg and Al-3at.%Cu alloys represent Al alloys that are relatively "simpler" in terms of their elemental composition. Experiments produced using these two alloys enable one to gather reactional information about the alloying elements from the two extremes of reactivity with significantly less interference from the other alloying elements rendering the interpretation of the acquired results relatively straightforward. With those data at hand, investigation of a more complex alloy, chemical composition-wise, with a similar set of experiments as for those "simpler" alloys was performed on AA7449-T651 alloy. The results are once again compiled in Figure 6.

Selective dissolution of Cu, Mg, and Zn was observed during the acid pickling surface treatment and sustained throughout the experiment once again as was the case for the simpler alloys. The rate of dissolution of Al during this pickling process was relatively stable at around 7 nmol s^{-1}, within the range of values found for Al in Al-3at.%Mg and Al-3at.%Cu for the same surface treatment process. The elemental depth profiles, on the other hand, might suggest that the alloying elements were enriched on the near-surface. One possible explanation for this could be that the pickling treatment was aggressive enough to remove the topmost layer and therefore underlying bulk metal was made closer to the surface compared to the unpickled bare surface.

The dissolution rate of Al for the directly converted surface (ZrCC) seemed to be within the same range as for Al-3at.%Mg and Al-3at.%Cu. The Al dissolution rate of the previously acid-pickled surface (NSFe-ZrCC) however appeared to be slightly higher throughout the whole conversion process. As for Al-3at.%Mg, Mg underwent selective dissolution during the process on the bare surface but dissolved congruently for the prior acid-pickled surface. Zn appeared to be dissolving non-preferentially during the Zr-conversion coating on the substrate's bare surface whereas during the same treatment process on a prior acid-pickled surface, the rate started to increase after around 300 s. The dissolution rates of Cu during this surface treatment process appeared to be higher than those found for the same element in Al-3at.%Cu, in addition to projecting a highly perturbed (noisy) signal albeit having an excellent detection limit.

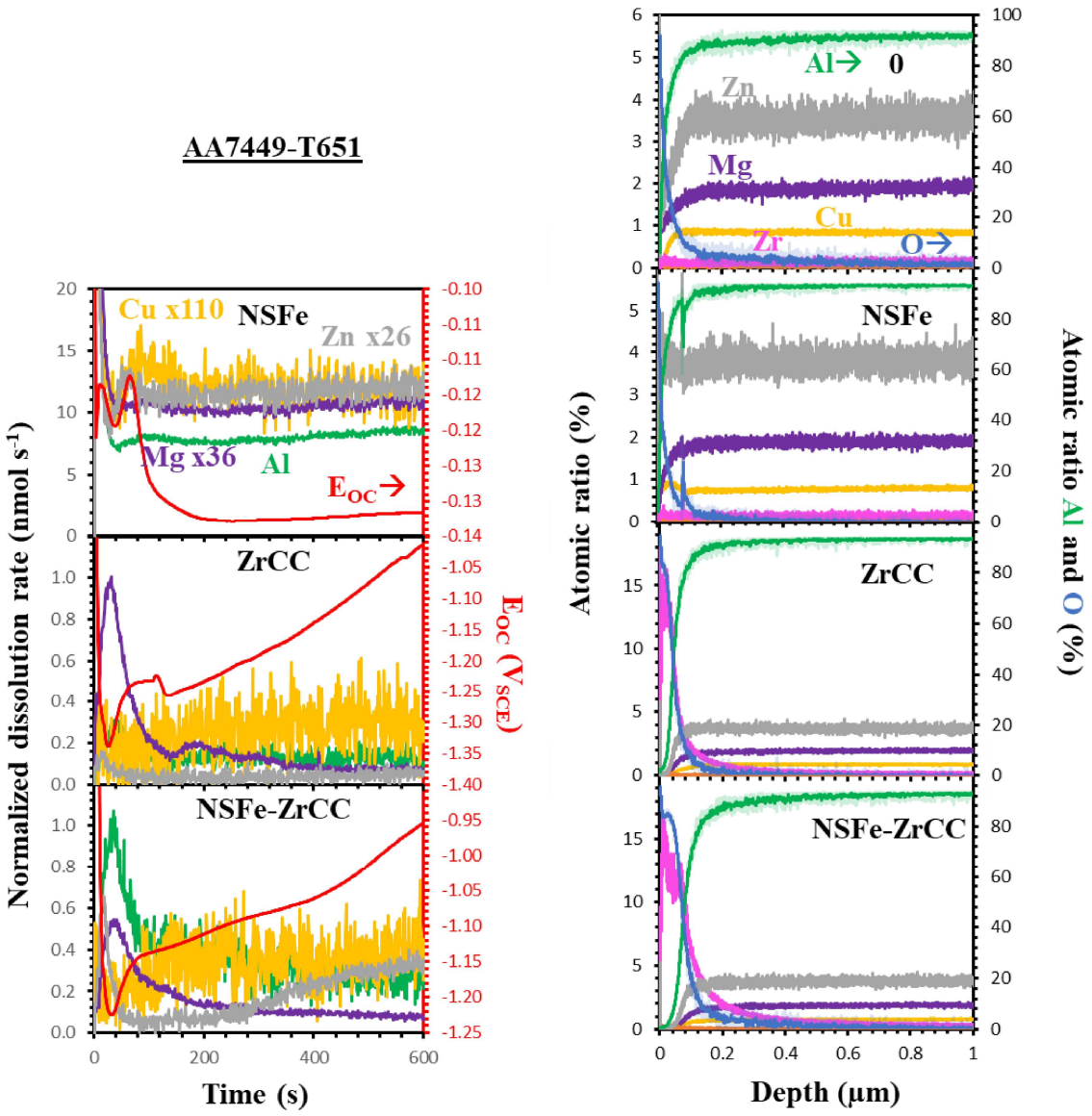

Figure 6 Left column: Normalized AESEC dissolution profiles of AA7449-T651 during acid pickling and the corresponding open circuit potential variation as a function of time during different surface treatment steps ─ during nitro-sulfuro-ferric (NSFe) acid pickling, and during Zr-conversion coating of bare (ZrCC) and benchtop acid pickled (NSFe-ZrCC) surfaces. Right column: Calibrated GD-OES elemental depth profiles of the corresponding surfaces after each surface treatment step compared with the bare surface (denoted as 0). Note that the atomic percentage of surface Al and O is given on the right-hand side y-axes.

Pertaining to elemental depth profile, the quantity of Zr appeared to be greater on the NSFe-ZrCC surface than on the ZrCC one as although the peak happened to be of similar percentage and the Zr on the NSFe-ZrCC surface was seen to be extended deeper (Figure 7). A similar observation was also noted for O. Another noteworthy observation was that the quantity of Zr approached zero sooner depth-wise compared to the previous two simpler alloys, indicating perhaps that the conversion layer was thinner on this complex alloy.

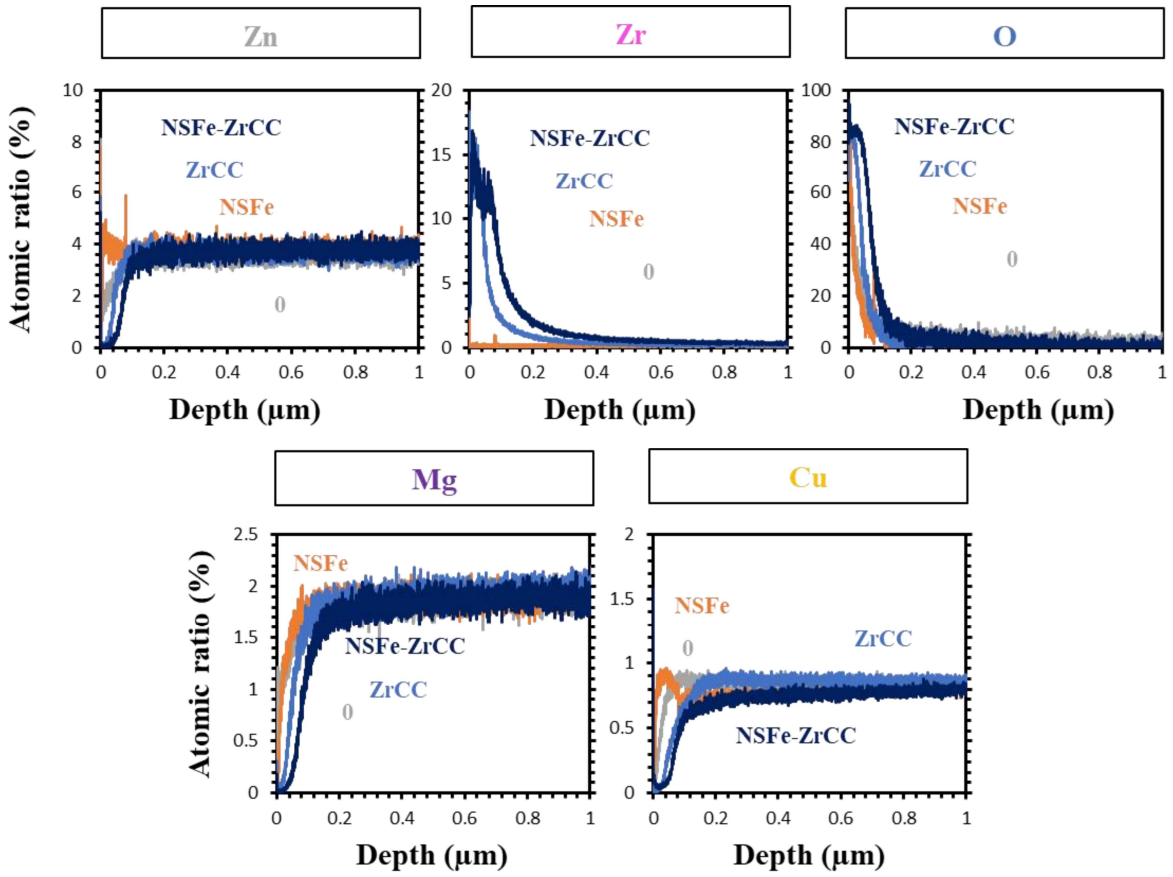

Figure 7 Calibrated individual elemental GD-OES depth profiles of Zn, Cu, Mg, Zr, and O of the surfaces after each surface treatment step superposed together for easier comparison of AA7449-T651. For reference, 0 denotes bare surface, NSFe signifies surface after acid pickling in nitro-sulfuro-ferric acid, ZrCC refers to bare surface after Zr-conversion coating, and NSFe-ZrCC represents NSFe surface after Zr-conversion coating.

d) Effect of additives – Fluoride

The effect of incorporating a few additives in the conversion coating solution bath was explored, however, since each additive has a specific hypothetical effect on the elementary processes, their individual effect needs to be confirmed first before rationalizing their overall effect in the conversion coating bath solution. Therefore, the first additive tested, F^- ion was added as NaF. A first set of experiments was performed on the simpler alloys (Al-3at.%Mg and Al-3at.%Cu) with just the NaF salt solution at concentrations of 50 and 100 mM at 50 °C and at pH 4.0 to observe F^-'s effect with minimal other interfering or synergistic effects. The acquired results are shown in Figure 8.

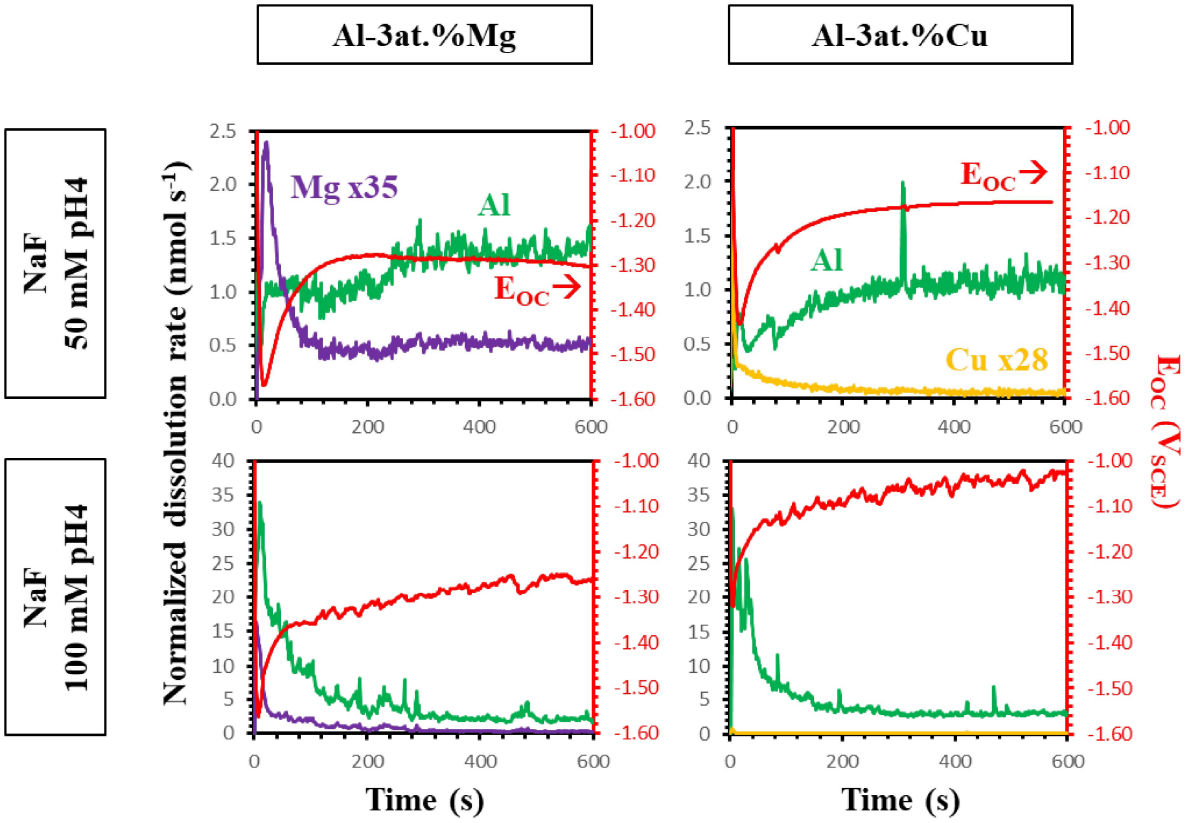

Figure 8 Normalized AESEC dissolution profiles and the corresponding potential evolution of Al-3at.%Mg (left column) and Al-3at.%Cu (right column) as a function of time during exposure to the NaF solution at concentrations of 50 (top row) and 100 (bottom row) mM, controlled at 50 °C and pH 4.

For the Al-3at.%Mg alloy, the dissolution rates of Al and Mg seemed to stabilize after 300 s in the solution with the lower concentration of F^- (50 mM) whereas in the higher concentration solution (100 mM), no apparent stabilization was observed. The same observation was also exhibited by the potential change. After a slight initial selective dissolution of Mg in 50 mM of F^- solution, Mg turned to undergo non-selective dissolution, probably owing to a passivation effect due to the formation of insoluble MgF_2 compound [26,27]. At a higher concentration of 100 mM, even the initial selective dissolution peak of Mg was not seen, and at the end of the experiment, the dissolution rate of this same element was even lower than the case in 50 mM. The effect on Al on the other hand was the opposite in such a way that a higher concentration of F^- enhanced considerably the rate of its dissolution. This can be attributed to the well-known effect of F^- on Al and Al oxide dissolution [28].

A similar occurrence in regard to Al was noted using the Al-3at.%Cu alloy. Cu, however, did not show significant change or differences when exposed to either concentration of F^-.

e) Effect of additives – Nitrate

Another common additive for commercial conversion coating bath solutions is NO_3^-. A similar set of experiments as the previous additive F^- were done with NO_3^- from $NaNO_3$ solution, again at 50 and 100 mM. Figure 9 reveals the results of this set of experiments.

The measured dissolution rates of Al in the presence of NO_3^- alone were barely above the detection limit for this element in 50 mM $NaNO_3$ solution (Table 2). The effect on Mg in Al-3at.%Mg alloy was observed to be indifferent to the concentrations of NO_3^- and probably influenced mostly by the pH of the solution instead (pH of the solution was adjusted by adding sulfuric acid). The evolution of the open circuit potential of Al-3at.%Mg alloy is consistent with the passivation of the surface after around 300 s, an effect not observed for the Al-3at.%Cu cases.

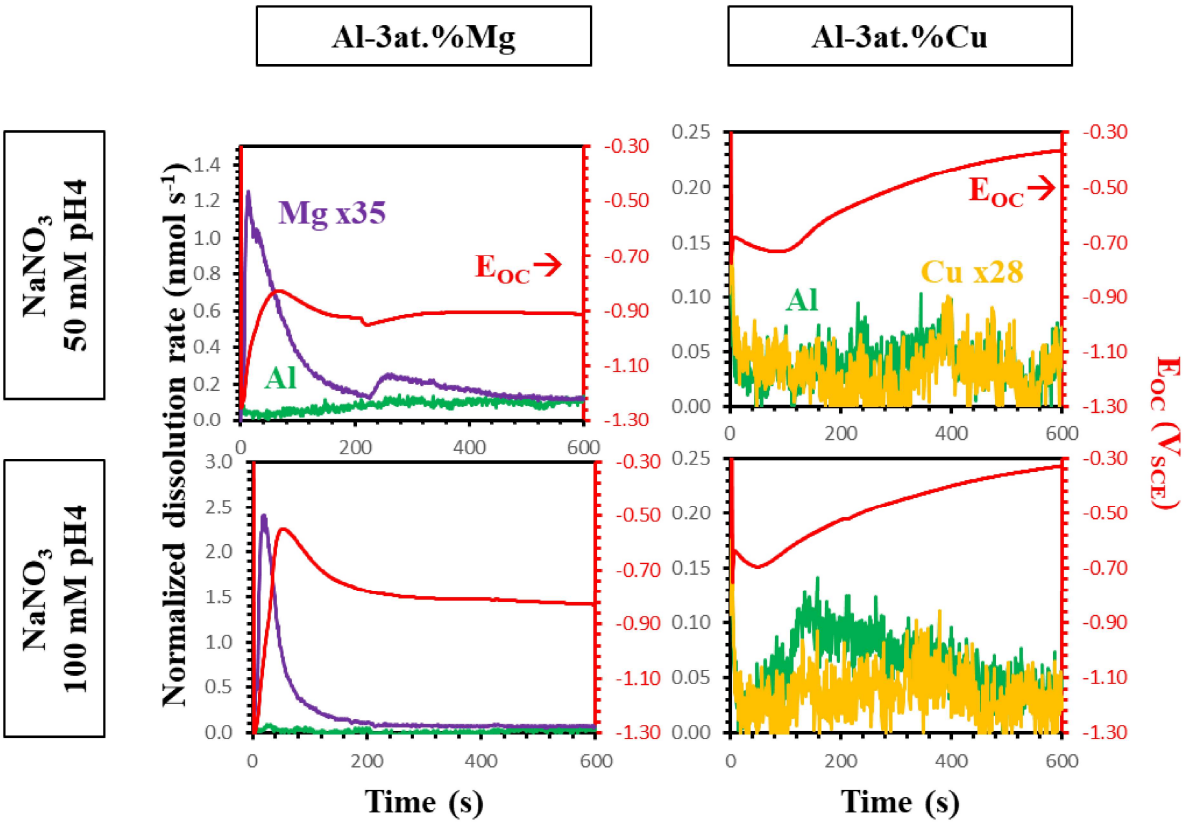

Figure 9 Normalized AESEC dissolution profiles and the corresponding potential evolution of Al-3at.%Mg (left column) and Al-3at.%Cu (right column) as a function of time during exposure to the $NaNO_3$ solution at concentrations of 50 (top row) and 100 (bottom row) mM, controlled at 50 °C and pH 4.0.

The dissolution rates of both Al and Cu in Al-3at.%Cu were relatively low and congruent after 300 s in 100 mM $NaNO_3$ solution. The potential also varied in a similar trend for both cases.

This lack of change might suggest that the concentrations of NO_3^- ions tested without the presence of other reactive species in the bath solution suggest that the pre-existing oxide layer needs to be removed or attacked before the influence of NO_3^- becomes fully apparent.

f) Zr-conversion coating with additives

Once the individual or isolated effects of F^- and NO_3^- on the dissolution kinetics of Al, Mg, and Cu were investigated at a glance, their influence in a proper conversion coating bath was probed on Al-3at.%Cu alloy by adding into the ZrCC bath solution 50 mM of either additive (F^- or NO_3^-) and the results were compared with the case without any additives in Figure 10.

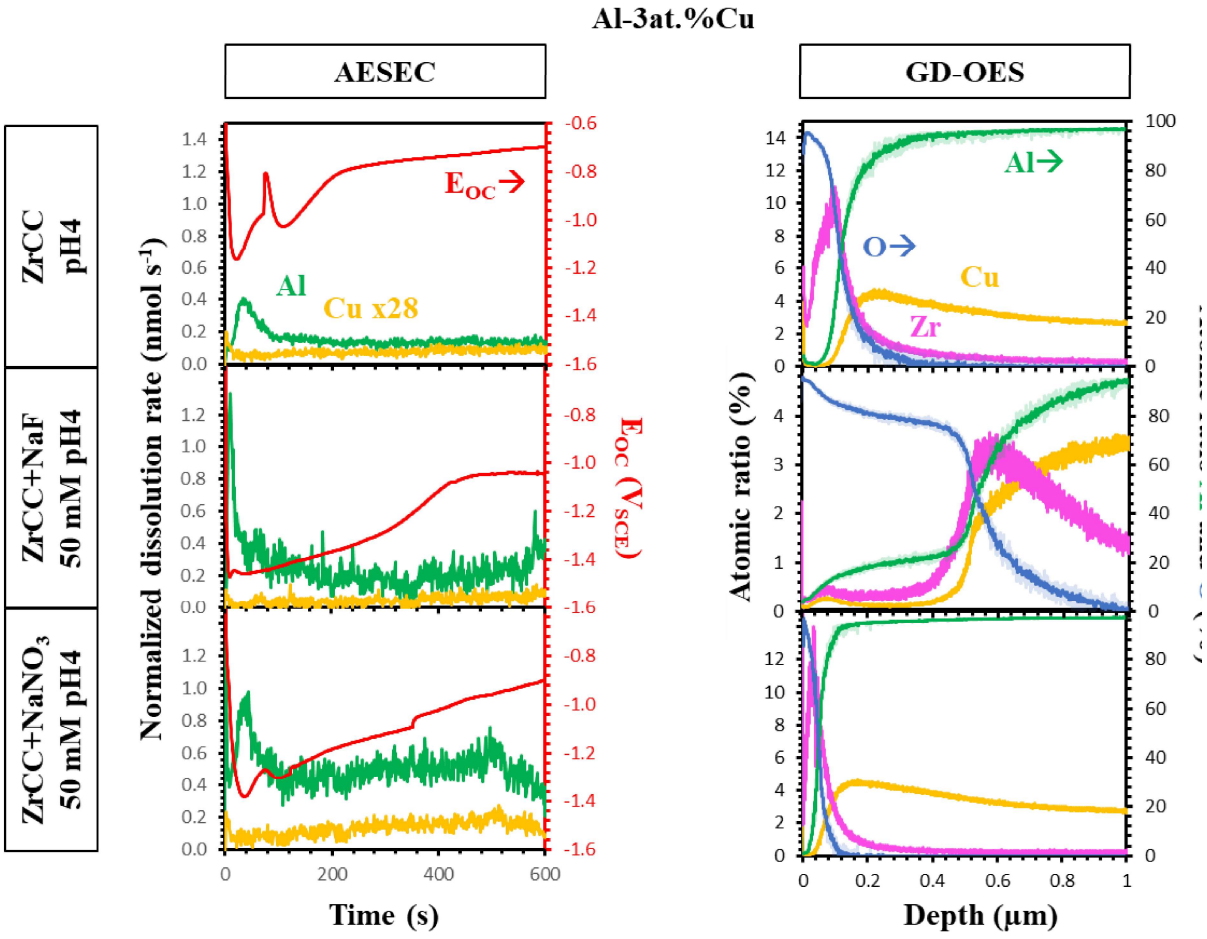

Figure 10 Normalized AESEC dissolution profiles and the corresponding potential evolution of Al-3at.%Cu as a function of time during exposure Zr-conversion coating process without additive (top, same data as in Figure 3-ZrCC), with the addition of 50 mM of NaF (middle), and with the incorporation of 50 mM of the $NaNO_3$ (bottom) at 50 °C and pH 4.0.

The open circuit potential (E_{OC}) versus time profile showed a similar trend in all cases ─ first the anodic dip followed by a slow rise to a steady state potential. The time required to reach a steady state increased in the order: ZrCC < ZrCC-F^- < ZrCC-NO_3^-.

Furthermore, the dissolution of Al was clearly enhanced in the presence of either additive, while that of Cu was higher with NO_3^- but lower with F^- as compared to the bath solution with no additives.

GD-OES analyses (Figure 10's right column and Figure 11) revealed that the ZrCC-NaF exhibited a thicker (around 400 nm) oxide layer on the topmost surface which is not attributable to either the oxides of Al, Cu, or Zr. ZrCC-$NaNO_3$ seemed to presumably possess a thinner but more homogeneous Zr-oxide layer compared to both ZrCC and ZrCC-NaF surfaces due to a narrower but more intense peak of Zr.

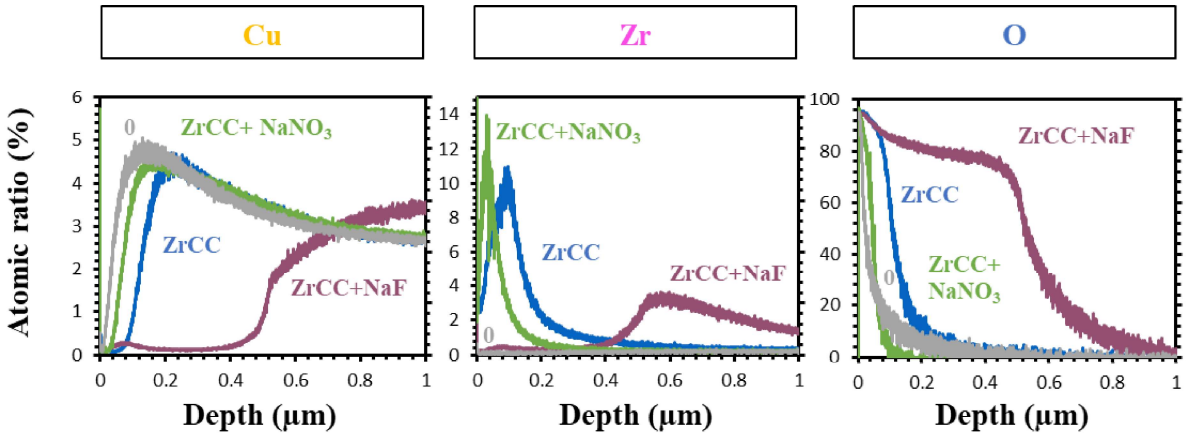

Figure 11 Calibrated individual elemental GD-OES depth profiles of Mg, Zr, and O of the surfaces after different conversion coating solution bath treatment superposed together for easier comparison of Al-3at.%Cu. For reference, 0 denotes bare surface, ZrCC refers to bare surface after Zr-conversion coating, ZrCC+NaF represents bare surface after Zr-conversion coating with the presence of 50 mM NaF, and ZrCC+$NaNO_3$ stands for bare surface after Zr-conversion coating with the presence of 50 mM $NaNO_3$.

4) Conclusion

The effect of acid pickling in nitro-sulfuro-ferric acid was investigated prior to Zr-based conversion coating surface treatment on alloy substrates, specifically Al-3at.%Mg, Al-3at.%Cu, and AA7449-T651. The key findings are as follows:

- **Selective Dissolution During Pickling:** Acid pickling selectively dissolved Mg and Cu, resulting in their surface depletion, as shown by GD-OES.
- **Dissolution and Deposition in Zr-Based Conversion Coatings:** Zr-based conversion coatings had significantly lower dissolution rates compared to acid pickling, with

greater Zr deposition on pre-pickled Al-3at.%Mg, Al-3at.%Cu, and AA7449-T651 alloys.

- **Conversion Layer Growth:** FT-IRRAS data indicated that longer Zr-based conversion treatments increased the conversion layer's quantity, though Al_2O_3 growth leveled off after 180 seconds.
- **F^- and NO_3^- Ion Effects:** Non-acid-pickled surfaces showed higher F^- content in ZrCC layers. F^- ions' impact on Al dissolution was concentration-dependent, whereas Mg and Cu were less affected. NO_3^- ions increased Al and Cu dissolution rates when added to the Zr-coating bath.
- **Surface Characteristics with Additives:** ZrCC with NO_3^- resulted in thinner, homogeneous Zr-oxide layers, while F^- produced thicker, complex oxides needing further study.

In conclusion, the influence of acid pickling prior to Zr-based conversion coating is significant. The role of specific additives and their effects on dissolution kinetics and final deposition quantity were highlighted. This information, combined with existing data, should aid in the smarter design of surface treatment protocols and bath solutions.

5) Contributions of Authors (CRediT)

B. Bin Mohamad Sultan – Conceptualization, Investigation, Methodology, Visualization, Writing - Original Draft, Writing - Review & Editing

D. Persson – Conceptualization, Visualization, Writing - Review & Editing

D. Thierry – Conceptualization, Writing - Review & Editing, Supervision, Funding acquisition

J.Han – Conceptualization, Methodology, Writing - Review & Editing

K. Ogle – Conceptualization, Methodology, Writing - Review & Editing, Supervision, Funding acquisition.

6) Acknowledgement

The authors would like to thank the *Agence National Recherche Technologie* (ANRT) and the *Agence Nationale de Recherche* (ANR) under grant #ANR-22CE08-0015-01 (QUEENE) for partial financing; Dr. Patrick Chapon of Horiba European Research Center for assistance and useful discussions concerning the GD-OES experiments respectively.

7) Annexes

To verify that the synthetic Zr-conversion coating bath solution produced in the laboratory can serve as a simpler alternative to commercial solutions, FT-IRRAS measurements were conducted for comparison, as shown in Figure .

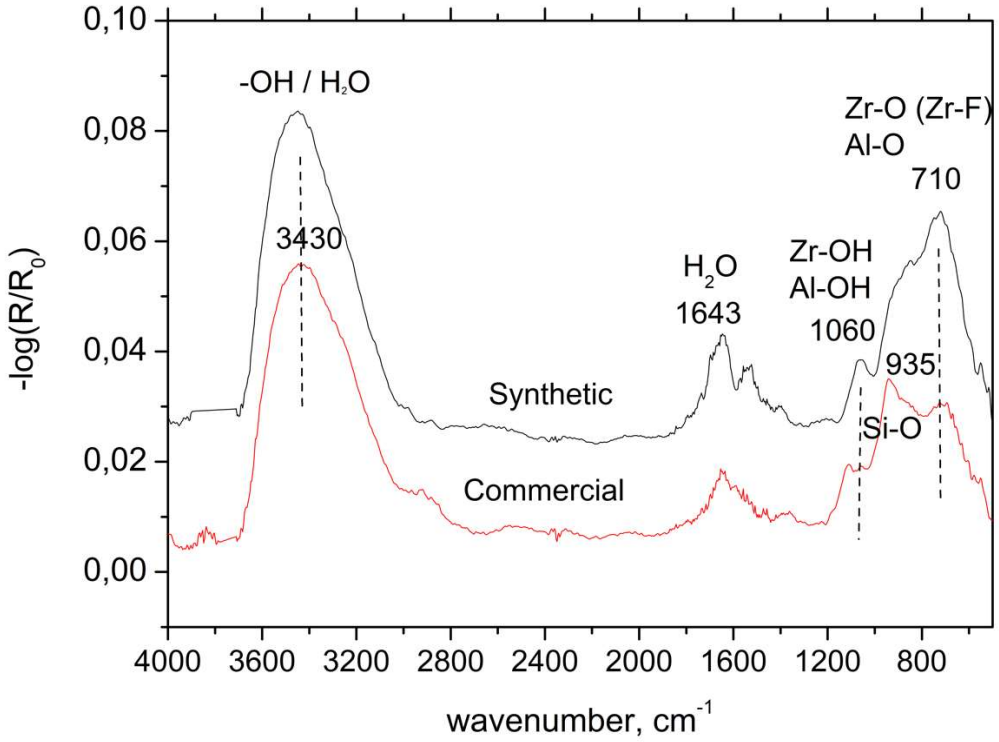

Figure A1 FT-IRRAS data comparing the mirror-polished surface of AlCu after being treated with a commercial Zr-based conversion coating solution and synthetic formulation used in this study (ZrCC). In either solution, the treatment duration was 3 min.

8) References

[1] G. Šekularac, J. Kovač, I. Milošev, Comparison of the Electrochemical Behaviour and Self-sealing of Zirconium Conversion Coatings Applied on Aluminium Alloys of series 1xxx to 7xxx, J Electrochem Soc 167 (2020) 111506. https://doi.org/10.1149/1945-7111/aba875.

[2] J. Han, D. Thierry, K. Ogle, Zr-based conversion coating on Zn and Zn-Al-Mg alloy coating: Understanding the accelerating effect of Cu(II) and NO3−, Surf Coat Technol 402 (2020) 126236. https://doi.org/10.1016/j.surfcoat.2020.126236.

[3] S.S. Golru, M.M. Attar, B. Ramezanzadeh, Morphological analysis and corrosion performance of zirconium based conversion coating on the aluminum alloy 1050, Journal of Industrial and Engineering Chemistry 24 (2015) 233–244. https://doi.org/10.1016/j.jiec.2014.09.036.

[4] S. Sharifi Golru, M.M. Attar, B. Ramezanzadeh, Effects of surface treatment of aluminium alloy 1050 on the adhesion and anticorrosion properties of the epoxy coating, Appl Surf Sci 345 (2015) 360–368. https://doi.org/10.1016/j.apsusc.2015.03.148.

[5] O. Gharbi, K. Ogle, J. Han, On the chemistry of the conversion coatings, in: Reference Module in Chemistry, Molecular Sciences and Chemical Engineering, Elsevier, 2023. https://doi.org/10.1016/B978-0-323-85669-0.00091-X.

[6] I. Milošev, G.S. Frankel, Review—Conversion Coatings Based on Zirconium and/or Titanium, J Electrochem Soc 165 (2018) C127–C144. https://doi.org/10.1149/2.0371803jes.

[7] G. Šekularac, I. Milošev, Electrochemical Behavior and Self-Sealing Ability of Zirconium Conversion Coating Applied on Aluminum Alloy 3005 in 0.5 M NaCl Solution, J Electrochem Soc 167 (2020) 021509. https://doi.org/10.1149/1945-7111/ab6b0d.

[8] G. Šekularac, J. Kovač, I. Milošev, A Prolonged protection, by zirconium conversion coatings, of AlSi7Mg0.3 aluminium alloy in chloride solution, Corros Sci 169 (2020) 108615. https://doi.org/10.1016/j.corsci.2020.108615.

[9] O. Gharbi, S. Thomas, C. Smith, N. Birbilis, Chromate replacement: what does the future hold?, Npj Mater Degrad 2 (2018) 23–25. https://doi.org/10.1038/s41529-018-0034-5.

[10] C.F. Glover, M.L.C. Lim, J.R. Scully, The Effect of Surface Treatment on the Performance of a Zirconium-Based Conversion Coating on AA7075 Automotive Alloys for Protection Against Filiform Corrosion, in: Minerals, Metals and Materials Series, 2020: pp. 937–946. https://doi.org/10.1007/978-3-030-36296-6_87.

[11] M. Becker, Chromate-free chemical conversion coatings for aluminum alloys, Corrosion Reviews 37 (2019) 321–342. https://doi.org/10.1515/corrrev-2019-0032.

[12] C.F. Glover, M.L.C. Lim, J.R. Scully, Increased Filiform Corrosion Resistance Utilizing a Zirconium-Based Conversion Coating on an Al-Zn-Mg-Cu (AA7075-T6) Alloy as well as Selected Surface Treatments, Corrosion 77 (2021) 40–52. https://doi.org/10.5006/3510.

[13] E. Mysliu, K. Sletteberg Storli, H.M. Skogøy, S. Kubowicz, I.H. Svenum, O. Lunder, A. Erbe, Effect of Cu2+ on deposition mechanism and structure of ZrO2-based conversion coatings on AA6060 aluminium alloys and their susceptibility to filiform corrosion, Electrochim Acta 477 (2024) 143805. https://doi.org/10.1016/J.ELECTACTA.2024.143805.

[14] J. Cerezo, I. Vandendael, R. Posner, K. Lill, J.H.W. de Wit, J.M.C. Mol, H. Terryn, Initiation and growth of modified Zr-based conversion coatings on multi-metal surfaces, Surf Coat Technol 236 (2013) 284–289. https://doi.org/10.1016/j.surfcoat.2013.09.059.

[15] Z. Bao, Q. Hu, W. Qi, Y. Tang, W. Wang, P. Wan, J. Chao, X.J. Yang, Nitrate reduction in water by aluminum alloys particles, J Environ Manage 196 (2017) 666–673. https://doi.org/10.1016/j.jenvman.2017.03.080.

[16] Z. Ahmad, Recent trends in processing and degradation of aluminium Alloys, InTech, 2011. https://doi.org/10.5772/741.

[17] K. Ogle, Atomic emission spectroelectrochemistry: A new look at the corrosion, dissolution and passivation of complex materials, Corrosion and Materials 37 (2012) 58–65.

[18] K. Ogle, Atomic Emission Spectroelectrochemistry: Real-Time Rate Measurements of Dissolution, Corrosion, and Passivation, Corrosion 75 (2019) 1398–1419. https://doi.org/10.5006/3336.

[19] J.E. Sansonetti, W.C. Martin, Handbook of Basic Atomic Spectroscopic Data, J Phys Chem Ref Data 34 (2005) 1559–2259. https://doi.org/10.1063/1.1800011.

[20] B.B.M. Sultan, D. Thierry, J.M. Torrescano-Alvarez, K. Ogle, Selective dissolution during acid pickling of aluminum alloys by element-resolved electrochemistry, Electrochim Acta 404 (2022) 139737. https://doi.org/10.1016/j.electacta.2021.139737.

[21] B.B.M. Sultan, D. Thierry, K. Ogle, On the dissolution rates and mechanisms of Al-Mg and Al-Cu alloys during acid pickling using element-resolved electrochemistry, Electrochim Acta 444 (2023). https://doi.org/10.1016/j.electacta.2023.141961.

[22] K. Wagatsuma, K. Hirokawa, N. Yamashita, Detection of fluorine emission lines from Grimm-type glow-discharge plasmas — use of neon as the plasma gas, Anal Chim Acta 324 (1996) 147–154. https://doi.org/10.1016/0003-2670(95)00623-0.

[23] L.F. Olbrich, A.W. Xiao, M. Pasta, Conversion-type fluoride cathodes: Current state of the art, Curr Opin Electrochem 30 (2021) 100779. https://doi.org/10.1016/J.COELEC.2021.100779.

[24] M. Itagaki, M. Tagaki, T. Mori, K. Watanabe, Active dissolution mechanisms of copper in acidic solutions containing sodium fluoride, Corros Sci 38 (1996) 601–610. https://doi.org/10.1016/0010-938X(95)00149-E.

[25] F.D. Speck, S. Cherevko, Electrochemical copper dissolution: A benchmark for stable CO2 reduction on copper electrocatalysts, Electrochem Commun 115 (2020) 106739. https://doi.org/10.1016/J.ELECOM.2020.106739.

[26] M.D. Pereda, C. Alonso, L. Burgos-Asperilla, J.A. del Valle, O.A. Ruano, P. Perez, M.A. Fernández Lorenzo De Mele, Corrosion inhibition of powder metallurgy Mg by fluoride treatments, Acta Biomater 6 (2010) 1772–1782. https://doi.org/10.1016/J.ACTBIO.2009.11.004.

[27] J. zhong LI, J. gui HUANG, Y. wen TIAN, C. sheng LIU, Corrosion action and passivation mechanism of magnesium alloy in fluoride solution, Transactions of Nonferrous Metals Society of China 19 (2009) 50–54. https://doi.org/10.1016/S1003-6326(08)60227-7.

[28] K.C. Walton, Effect of fluoride on the amount of aluminium dissolved by boiling fruit acids, Environmental Pollution 60 (1989) 223–233. https://doi.org/10.1016/0269-7491(89)90106-1.